Strain compensated type II superlattices grown by molecular beam epitaxy

Chao Ning(宁超)[1,2], Tian Yu(于天)[1,2], Rui-Xuan Sun(孙瑞轩)[1,2], Shu-Man Liu(刘舒曼)[1,2,†], Xiao-Ling Ye(叶小玲)[1,2], Ning Zhuo(卓宁)[1,2,‡], Li-Jun Wang(王利军)[1,2], Jun-Qi Liu(刘俊岐)[1,2], Jin-Chuan Zhang(张锦川)[1,2], Shen-Qiang Zhai(翟慎强)[1,2], and Feng-Qi Liu(刘峰奇)[1,2,3]

[1] *Key Laboratory of Semiconductor Materials Science, Institute of Semiconductors, Chinese Academy of Sciences, Beijing* 100083, *China*
[2] *Center of Materials Science and Optoelectronics Engineering, University of Chinese Academy of Sciences, Beijing* 100049, *China*
[3] *Beijing Academy of Quantum Information Sciences, Beijing* 100193, *China*

(Received 25 April 2022; revised manuscript received 22 June 2022; accepted manuscript online 29 June 2022)

We investigate a strain compensation method for the growth of complex interband cascade laser structures. For thick InAs/AlSb superlattice clad layers, the sublayer thicknesses were adjusted so that the tensile strain energy in the InAs sublayer was equal to the compressive strain energy in the AlSb sublayer. For the four-constituent active region, as the compressive strain in the $Ga_{0.65}In_{0.35}Sb$ alloy layer was large, a tensile strain was incorporated in the chirped InAs/AlSb superlattice region for strain compensation to the $Ga_{0.65}In_{0.35}Sb$ alloy. A laser structure of thickness 6 μm was grown on the GaSb substrate by molecular beam epitaxy. The wafer exhibited good surface morphology and high crystalline quality.

Keywords: type-II superlattices, strain compensation, molecular beam epitaxy

PACS: 68.65.Cd, 61.72.uj, 81.15.Hi **DOI:** 10.1088/1674-1056/ac7cd4

1. Introduction

InAs/AlSb and InAs/Ga(In)Sb type II superlattices have been widely used in various optoelectronic devices, such as interband cascade lasers,[1] quantum cascade lasers,[2] mid-IR diode lasers[3,4] and infrared photodetectors.[4–6] Since for InAs/AlSb superlattices there are no common atoms in the two layers, both III and V species have to be exchanged at the interfaces. The quality of an interface is affected by atomic diffusion from both sides of the interface and the incorporation efficiency of background group V species. Furthermore, because the lattice constants of InAs and AlSb are different from that of the GaSb substrate there is strain in the epitaxial superlattice. Strain-balanced InAs/AlSb superlattices on GaSb substrates could be achieved theoretically by almost equal InAs and AlSb sublayer thicknesses since there are relative mismatches of −0.62% and +0.65% in InAs and AlSb sublayers, respectively, to the GaSb substrate. However, atomic diffusion is prone to occur on non-common atomic interfaces.[7–10] In addition, Al–As bonds are stronger than Al–Sb bonds, which might cause As to enter the AlSb layer[11] and change the net strain in the superlattice. These issues might affect the structural quality of thick InAs/AlSb superlattices.

Although there have been reports on the optimization of the growth parameters of molecular beam epitaxy (MBE) for type II antimonide quantum wells (QWs) in the past 20 years,[12–19] such as substrate temperatures, interfacial bond types and V/III beam equivalent pressure (BEP) ratios, it is still challenging to grow high-quality type II antimonide superlattices with thousands of sublayers. In this work, we report an analysis of the accumulation of strain energy in InAs/AlSb and InAs/GaInSb type II superlattices. A strain compensation method is proposed based on the balance between tensile and compressive strain energy. A superlattice interband cascade laser structure consisting of InAs, AlSb, GaInSb and GaSb sublayers was grown according to this strain compensation method. The epilayer exhibited a smooth surface morphology.

2. Theory

The mismatch f and strain ε_0 between an epitaxial layer and the substrate can be described respectively by

$$f = \frac{a_s - a_l}{a_s}, \tag{1}$$

$$\varepsilon_0 = \frac{a_s - a_l}{a_l}, \tag{2}$$

where a_s and a_l are the equilibrium lattice constants of substrate and epilayer materials, respectively. A coherently grown epitaxial layer with the zinc blende structure is subjected to isotropic biaxial stress parallel to the substrate surface. According to Hooke's law, the in-plane stress $\sigma_{\parallel}$ is described by

$$\sigma_{\parallel} = 2G\frac{1+\nu}{1-\nu}\varepsilon_0, \tag{3}$$

where ν is the Poisson's ratio and G is the shear modulus of the epitaxial layer.

†Corresponding author. E-mail: liusm@semi.ac.cn
‡Corresponding author. E-mail: zhuoning@semi.ac.cn

© 2023 Chinese Physical Society and IOP Publishing Ltd

The in-plane stress of the epitaxial layer produces elastic strain energy, and the energy density $E_{\parallel}$ can be expressed as

$$E_{\parallel} = 2G\frac{(1+\nu)}{(1-\nu)}h\varepsilon_0^2, \tag{4}$$

where h is the thickness of the epilayer. The strain energy accumulated in the epitaxial layer is proportional to the thickness h and increases the system's free energy. When the epilayer is thicker than a critical value, further growth causes stress relaxation to lower the system's free energy, often accompanied by misfit dislocation networks. According to the Matthew–Blakeslee (M–B) formula,[20] the critical thickness h_c is calculated from

$$h_c = \frac{b(1-\nu\cos^2\theta)}{8\pi f(1+\nu)\cos\varphi}\ln\left(\frac{4h_c}{b}\right), \tag{5}$$

where b is the Burgers vector of a dislocation, which equals $a_s/\sqrt{2}$, θ is the angle between the dislocation line and the Burgers vector and φ is the angle between the slip direction and the projection of the slip direction on the epitaxial layer. In general, $\theta = \varphi = 60^\circ$.

Based on the work of Matthew and Blakeslee, People and Bean (P–B) proposed their formula from the perspective of energy minimization.[21,22] The P–B formula is as follows:

$$h_c = \frac{(1-\upsilon)b^2}{16\sqrt{2}\pi(1+\upsilon)a_s f^2}\left(\ln\frac{h_c}{b}\right). \tag{6}$$

The meaning of each symbol in the formula is the same as above. We calculated the critical thicknesses for InAs and AlSb heteroepitaxial layers grown on a GaSb substrate and GaSb and AlSb epilayers on an InAs substrate using the material parameters listed in Table 1. The results are listed in Table 2.

Table 1. Material parameters for the calculation of critical thicknesses.[23]

Materials	Lattice constant (Å)	C_{11} (GPa)	C_{12} (GPa)	C_{44} (GPa)	Strain on various substrates ε (%)	
InAs	6.0583	832.9	452.6	395.9	–	−0.62
GaSb	6.0959	884.2	402.6	432.2	0.62	–
AlSb	6.1355	876.9	434.1	407.6	1.26	0.65
InSb	6.4794	684.7	373.5	311.1	6.50	5.92
AlAs	5.6611	1250	534	542	−7.02	−7.68

Table 2. Critical thicknesses calculated from the M–B and P–B expressions for InAs, GaSb and AlSb hetero-epilayers.

Epilayer	InAs substrate		GaSb substrate	
	M–B h_c (Å)	P–B h_c (Å)	M–B h_c (Å)	P–B h_c (Å)
InAs	–	–	193.8	3595.3
GaSb	203.4	3962.6	–	–
AlSb	80.4	670.93	189.0	3401.9

The results calculated using Eqs. (5) and (6) are different. We grew a 100 nm thick InAs epitaxial layer on a GaSb substrate to see which one is consistent with experiments. The surface morphology of the sample is shown in Fig. 1(a). A series of parallel striped protrusions can be observed in a field of view of 30 μm × 30 μm; these are ascribed to misfit dislocations. They are along the step flow $(0\bar{1}1)$ direction of a two-dimensional (2D) growth mode. Most striped protrusions are 0.7 nm higher than the 2D grown surface, as indicated by the tip trace in Fig. 1(c), which is recorded along the solid line in Fig. 1(a). There is also a ∼ 1.4 nm high strip on the right of the image. More details can be observed at a 5 μm scale: the striped protrusions are composed of multiple atomic steps, which are part of the 2D step flow growth surface. There is a 100 nm wide trench in the center of each stripe, where atomic steps are visible. It is noted that a step edge AB along the stripe direction appears on the 2D grown surface and looks like a stacking fault. Figure 1(d) records the tip trace along the solid line in Fig. 1(b). The height difference between the two dots on both sides of the step edge AB is 0.15 nm, which is half the height of an InAs monolayer (ML).

Considering the above three striped features with the same direction but different heights, we speculate that the formation mechanism is as follows: when the epilayer is thicker than h_c, some steps of half a ML in height might form initially on the growth front to relax the stress in the epilayer. There should be large numbers of kink sites near such step edges, where the probability of atomic incorporation is higher than that on terraces formed by the normal step flow mode. Thus, striped protrusions might be formed during the subsequent growth process. With the deposition of InAs, the strain gradually accumulates and new half-ML high steps might be formed at the growth front to relax the stress, followed by striped protrusions near the step edges. The 100 nm thick InAs-on-GaSb sample exhibits the topographical features shown in Fig. 1. Thinner or thicker samples may show different strip heights and densities.

Since our growth experiment found misfit dislocations in 100 nm thick the InAs layer epitaxially grown on a GaSb substrate, the critical thickness $h_c = 359.5$ nm obtained by the P–B formula disagrees with the experiment. The deviation can be ascribed to the fact that the P–B formula was derived from the perspective of fully relaxed internal stress in the epitaxial layer. Under this assumption, there should be a dislocation network with a density of $\sim 10^5$ cm^{-1} in a fully relaxed InAs film. However, a lower dislocation density of $\sim 10^3$ cm^{-1} was observed by atomic force microscopy (AFM), suggesting residual stress in the epitaxial layer. Therefore, the critical thickness calculated from the M–B formula is more accurate for the GaSb/InAs epitaxial system.

According to the energy density expression (Eq. (4)), the rate of strain energy accumulation in an epilayer is $2G\frac{(1+\nu)}{(1-\nu)}\varepsilon_0^2$, which is 0.0636 GPa (0.0676 GPa) for an InAs (AlSb) epilayer

on a GaSb substrate. Similarly, the rate of strain energy accumulation for a GaSb (AlSb) epilayer on an InAs substrate is 0.0628 GPa (0.2568 GPa). Therefore, the accumulated energy density is less than 1.233 J·m^{-2} for a strained InAs layer grown on GaSb, and 1.277 J·m^{-2} for AlSb on GaSb; the accumulated energy density in a strained GaSb epilayer coherently grown on an InAs substrate is less than 1.277 J·m^{-2}, and is 2.065 J·m^{-2} for AlSb on InAs.

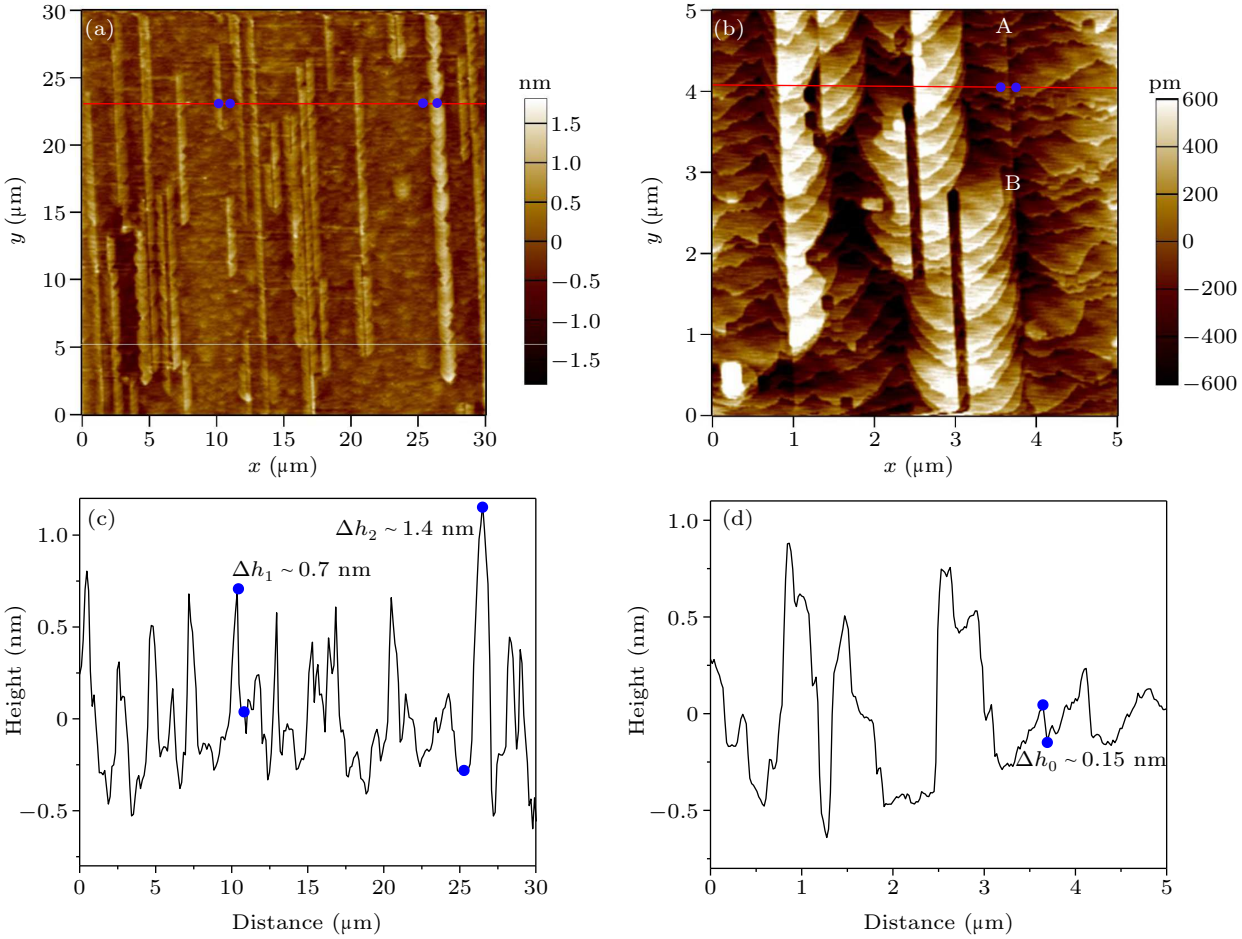


Fig. 1. Atomic force microscopy images for a 100 nm thick InAs film hetero-epilayer on a GaSb substrate with the scan range of (a) 30 μm × 30 μm and (b) 5 μm × 5 μm. (c) Height profile along the red line in panel (a). (d) Height profile along the red line in panel (b).

In a strain-compensated superlattice epilayer, the tensile and compressive strain sublayers are usually grown alternately, and the strain in each epitaxial sublayer repeatedly changes its sign. A common solution for strain compensation is to have the net strain as close to zero as possible.[9,15,24] Experimentally, the period and residual strain of an InAs/AlSb superlattice sample is usually deduced from high-resolution x-ray diffraction (HRXRD) measurements according to

$$2D\sin\theta_{\rm sub} = nN\lambda, \tag{7}$$

where N is the number of bilayers in the superlattice, $\theta_{\rm sub}$ is the Bragg angle of the GaSb substrate, n is diffraction order and D is the superlattice period. In general, the strain is considered to be completely compensated when the zeroth satellite peak of a superlattice overlaps with the substrate peak, which is expressed as follows:

$$\frac{d_{\rm InAs}\cdot N_{\rm InAs} + d_{\rm AlSb}\cdot N_{\rm AlSb}}{N_{\rm InAs} + N_{\rm AlSb}} = d_{\rm GaSb}. \tag{8}$$

The left-hand side is the weighted average of the lattice spacing d of InAs and AlSb. Under biaxial strain, the lattice spacing along the (001) direction turns to $d_{\rm InAs} = 6.0451$ Å, and $d_{\rm AlSb} = 6.1486$ Å, while $d_{\rm GaSb} = 6.0959$ Å is not affected by strain. Taking these three values and $N_{\rm InAs} = 3.8$ (corresponding to an InAs layer thickness of 23 Å) into Eq. (8), the thickness of the AlSb sublayer in a period should be 22.6 Å.

From the point of view of strain energy, we propose another strain compensation method in which the accumulated tensile strain energy in InAs equals the compressive strain energy in AlSb so that the net strain energy is zero. The strain energy density increases linearly with the layer thickness as described by Eq. (4), therefore the thicknesses of InAs and AlSb should satisfy the following relationship:

$$0.0636\ {\rm GPa}\cdot h_{\rm InAs} = 0.0672\ {\rm GPa}\cdot h_{\rm AlSb}. \tag{9}$$

Assuming the thickness of an InAs sublayer to be 23.0 Å, without considering the influence of the interface composition

on the strain energy density, we obtained the thickness of the AlSb sublayer to be 21.8 Å.

Note that when the thickness of InAs is fixed at 23 Å, the thickness of strain-compensated AlSb is calculated to be 22.6 Å by Eq. (8) and 21.8 Å by Eq. (9). The dynamically simulated x-ray diffraction (XRD) spectra of InAs (23 Å)/AlSb (21.8 Å) and InAs (23 Å)/AlSb (22.6 Å) superlattice structures on GaSb substrates are displayed in Figs. 2(a) and 2(b), respectively. An enlarged view near the GaSb peak is shown in the inset.

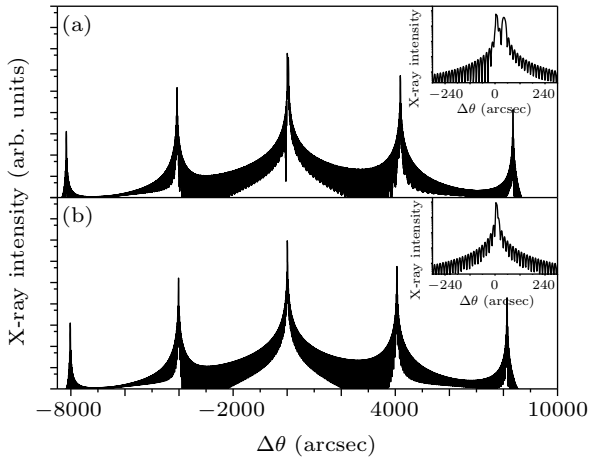


Fig. 2. (a) Dynamic simulation for an InAs (23 Å)/AlSb superlattice on a GaSb substrate with the AlSb thickness calculated according to (a) Eq. (9) and (b) Eq. (8). The insets show enlargements of the pattern around the GaSb substrate.

The position of the zeroth-order satellite peak of structure (a) differs from the GaSb peak by 41 arcsec, while the residual strain energy in this structure is close to zero. By comparison, the zeroth-order satellite peak of structure (b) overlaps with that of the GaSb substrate, and is given by the common lattice matching condition (Eq. (8)). However, there is net compressive strain energy of 0.00622 J·m^{-2} per period in this superlattice structure. Theoretically, strain relaxation may occur in superlattice structure (b) after the growth of 205 periods according to the AlSb critical thicknesses listed in Table 2.

As a certain amount of strain energy can remain in an epitaxial material without relaxation, we estimated the growth window of InAs/AlSb superlattices grown on a GaSb substrate according to such residual strain energy. The strain energy is E_{InAs} and E_{AlSb} in each constituent, and is positive for compressive AlSb and negative for tensile InAs. After the growth of one period, the change in the overall strain energy is $\Delta E = E_{\mathrm{InAs}} + E_{\mathrm{AlSb}}$. A positive ΔE represents net compressive strain energy, and vice versa. With the accumulation of tensile strain energy, the relaxation must start in the InAs layer, while compressive strain relaxation must occur in the AlSb layer. Therefore, the limit for maximum tensile and compressive strain energy accumulated in the superlattice corresponds to the strain energy of InAs and AlSb with the critical thickness, which is $-E_{\mathrm{c}}^{\mathrm{InAs}}$ and $E_{\mathrm{c}}^{\mathrm{AlSb}}$, respectively. For an N-period superlattice, the strain energy should satisfy the following relationship:

$$-E_{\mathrm{c}}^{\mathrm{InAs}} \le N \cdot (E_{\mathrm{AlSb}} + E_{\mathrm{InAs}}) \le E_{\mathrm{c}}^{\mathrm{AlSb}}. \tag{10}$$

In our interband cascade laser structures, the typical lower clad layer comprises a 600-repetition InAs (23 Å)/AlSb (21.8 Å) superlattice, then the strain energy per period is

$$\begin{aligned} -2.055 \times 10^{-3} \left(\mathrm{J/m^2}\right) &\le (E_{\mathrm{AlSb}} + E_{\mathrm{InAs}}) \\ &\le 2.128 \times 10^{-3} \left(\mathrm{J/m^2}\right). \end{aligned} \tag{11}$$

Hence, the tolerable deviation of the layer thickness in each unrelaxed period can be obtained by dividing the upper limits of strain energy by the respective accumulation rates as follows:

$$\begin{cases} -0.3231\ \text{Å} \le \Delta h_{\mathrm{InAs}} \le 0.3346\ \text{Å}, \\ -0.3040\ \text{Å} \le \Delta h_{\mathrm{AlSb}} \le 0.3148\ \text{Å}. \end{cases} \tag{12}$$

The period thickness deviation should be less than 1.40%. In other words, for a strain-compensated superlattice, the deviation of the growth rate should be less than 0.7%. We know that the growth rate of a binary III–V material is usually determined by the deposition rate of the group III metal, which is controlled by the cell temperature T. For our MBE system, the growth rate $R(T)$ has the following empirical expression:

$$R(T) = A\,\mathrm{e}^{(T-T_0)\cdot \ln 1.02}, \tag{13}$$

where A is a fitting constant and T_0 is the setpoint temperature.

If the growth rate fluctuates by 0.7%, i.e., it becomes ±100.7% of the set value, the cell temperature changes by ±0.35 °C according to Eq. (13). In short, to grow 600 repetitions of an InAs/AlSb superlattice on a GaSb substrate without strain relaxation, the temperature fluctuation of group III sources should be within ±0.35 °C.

3. Experiment and results

The growth rate is not only affected by fluctuations in cell temperature or beam flux but also by shutter motion. When a cell shutter opens or closes, the thermal balance in the crucible is disturbed, resulting in the so-called 'switching transient' which also affects the deposition rate. Specifically, as soon as a shutter opens, the temperature of the group III source drops immediately due to evaporation. At this moment, the PID controller increases the heating power instantaneously, causing the source temperature to overshoot. The instantaneous beam flux might be 10%–20% higher than the stable one. The influence of this flux transient on the growth of thick bulk materials is negligible; however, the shutters frequently open and close during the growth of short-period superlattices. Since it takes 10–15 s for the beam fluxes of group III elements to stabilize in our MBE machine and the growth time of each sublayer in our superlattice sample is about 20–30 s we estimate that 50%

of the growth is carried out in the switching transient, whose influence on the growth rate must be taken into account. If BEP is used to monitor the growth rate, one must calibrate carefully. Thus we determined the growth rate according to reflection high-energy electron diffraction (RHEED) oscillations instead of group III beam flux. Figure 3 shows a typical RHEED oscillation curve obtained from a two-period InAs (7 ML)/AlSb(8 ML) superlattice followed by a 10 ML GaSb layer. According to the position of the oscillation peak the average growth rate is 1 ML·s^{-1} for AlSb, 0.48 ML·s^{-1} for InAs and 0.5 ML·s^{-1} for GaSb.

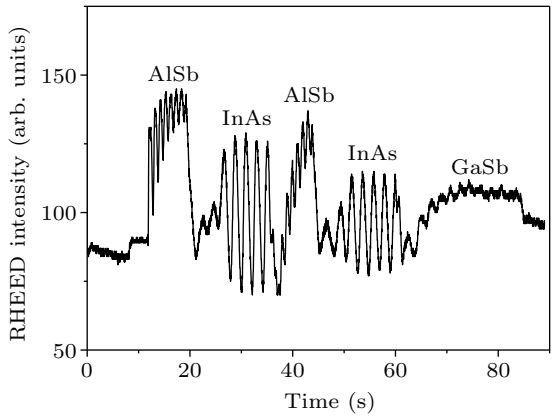


Fig. 3. RHEED intensity oscillation during the overgrowth of a two-period AlSb/InAs superlattice followed by 10 ML GaSb.

During the growth of InAs/AlSb superlattices, even though the valve and shutter of the As crack cell immediately closed at the end of InAs growth, the residual As in the growth chamber affected the following AlSb epitaxial layer significantly. This has been confirmed by the HRXRD pattern of a 150-period InAs (7.5 ML)/AlSb (7 ML) superlattice sample, as shown in the upper panel of Fig. 4(a).

The sample was grown using a V/III BEP ratio of 5:1 without a special shutter sequence on the interfaces. The zeroth-order satellite peak is found at 1498 arcsec, indicating that the out-of-plane lattice constant of the superlattice sample is smaller than that of GaSb. The red dashed curve is the result of a dynamic diffraction theory simulation. The was structure used for fitting is InAs/AlSb$_{0.835}$As$_{0.165}$ superlattice.

Although the wide bandgap AlAs constituent does not reduce the barrier height of AlSb, the mixing of such a large amount of AlAs with AlSb led to a rapid accumulation of tensile strain energy in the superlattice that eventually exceeded the critical value. We have observed many dislocations in this sample by transmission electron microscopy and AFM and as shown in Figs. 4(b) and 4(c), respectively.

We incorporated an Sb soak after InAs deposition to prevent As from mixing into the AlSb layer, as shown in Fig. 5(a). During the Sb soak, the proportion of Sb atoms adsorbed on the InAs surface increased and the background As pressure decreased, which reduced the probability of bonding between Al and As atoms in the consequent AlSb layer. We also found (1×3) RHEED patterns when the soak time was long enough, implying the establishment of an Sb-rich reconstruction on the InAs surface.

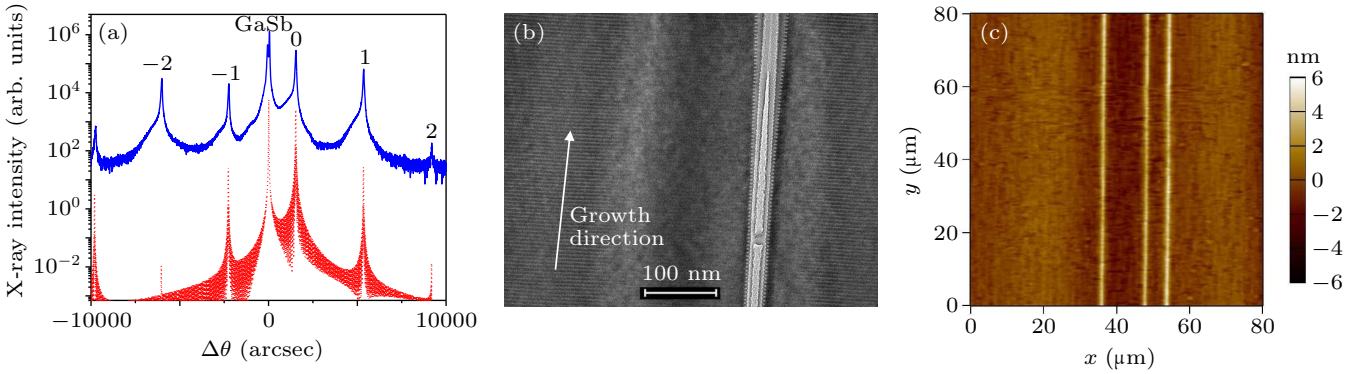


Fig. 4. (a) High-resolution x-ray diffraction spectrum and a dynamical simulation (red dashed line). (b) Transmission electron microscopy cross-section image. (c) AFM image for an InAs/AlSb superlattice grown on a GaSb substrate with natural interfaces.

Two InAs/AlSb superlattice samples were grown using Sb soak times of 3 s and 1 s, respectively. Figure 5 shows the XRD rocking curves. The zeroth-order satellite peak is at 880 arcsec for the superlattice sample with a 1 s Sb soak, suggesting a large lattice mismatch of the epilayer to the substrate. By comparison, the zeroth-order satellite peak is at 60 arcsec for the sample with a 3 s Sb soak, close to the peak position of 41 arcsec shown in Fig. 2(a) for the strain balanced structure. There is only a small amount of AlAs in the AlSb sublayer of the sample grown with a 3 s Sb soak. This indicates that the Sb-soak time of 3 s is sufficient to ensure the purity of the bulk AlSb sublayer.

So far, we have optimized the growth scheme for the 600-period strain-balanced InAs/AlSb superlattice clad layer by two means. On one hand, the thickness ratio of the InAs and AlSb layers is optimized for minimum net strain energy; on the other hand, the InAs surface is soaked with Sb for 3 s before deposition of AlSb.

For the InAs/GaInSb/InAs 'W' QW, the GaInSb ternary alloy composition dominates the strain of the epitaxial layer.

A high In composition produces high in-plane compressive strain, which splits the light- and heavy-hole bands. This splitting is beneficial to low Auger recombination rates. However, as the tensile strain created by thin InAs layers can hardly compensate for the high compressive strain in GaInSb, dislocations may form beyond a critical layer thickness.

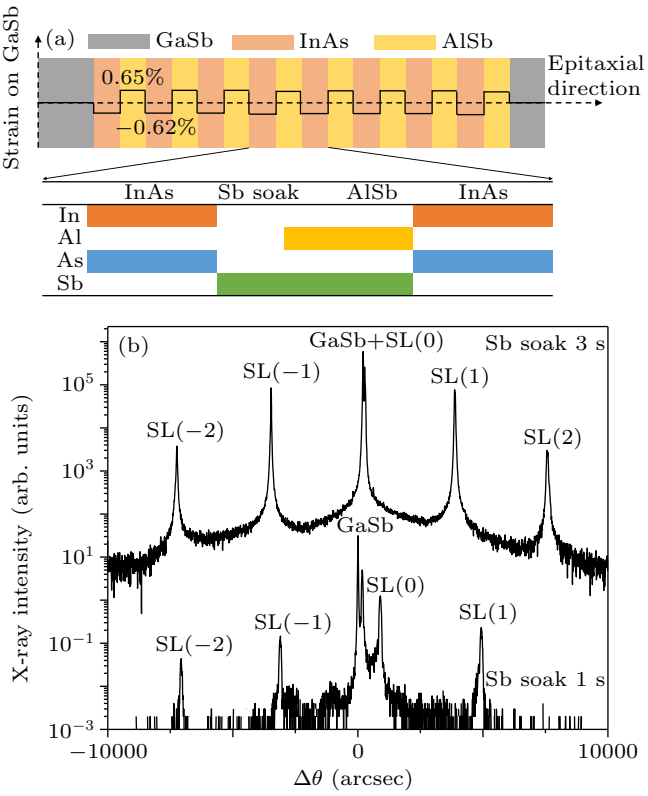


Fig. 5. (a) Schematic diagram of the growth of InAs/AlSb superlattices using an Sb soak. (b) High-resolution x-ray diffraction spectrum of an InAs/AlSb superlattice overgrown on a GaSb substrate with an Sb soak time of 1 s (lower panel) and 3 s (upper panel) for AlSb-on-InAs interfaces.

The growth rate of InGaSb ternary alloy is determined by In and Ga beam fluxes. As the mismatch between InSb and GaSb (InAs) substrates is as large as 5.92% (6.50%), the critical thickness of GaInSb decreases rapidly with increase in the InSb content.[25] Figure 6 compares the calculated M–B critical thicknesses of GaInSb epilayers on GaSb and InAs substrates as a function of In composition. The inset shows a partially enlarged view. On a GaSb substrate, the maximum In content reaches 42% for a 3 nm thick strained $Ga_{1-x}In_xSb$ layer. On an InAs substrate, the value is 33%.

The 'W' QWs were not grown directly on a GaSb buffer but on an InAs/AlSb superlattice in the laser structure, as shown by the schematic diagram in Fig. 7(a). Each active region consists of an InAs (17 Å)/$Ga_{0.65}In_{0.35}Sb$ (30 Å)/InAs (14 Å) 'W' quantum well, GaSb 45 Å/AlSb 10 Å/GaSb 30 Å/AlSb 10 Å hole injector and an AlSb 25 Å/InAs 18 Å/AlSb 12 Å/InAs 18 Å/AlSb 12 Å/InAs 20 Å/AlSb 12 Å/InAs 24 Å/AlSb 12 Å/InAs 27 Å/AlSb 12 Å/InAs 30 Å/AlSb 25 Å electron injector. As the compressive strain energy accumulated in the 30 Å thick $Ga_{0.65}In_{0.35}Sb$ layer is larger than the tensile energy in the two InAs thin layers in the 'W' QW, we introduce an appropriate tensile strain into the chirped superlattice to compensate for the compressive strain and reduce the total free energy. Figures 7(b) and 7(c) display the AFM images for a seven-period active region. The sample exhibits excellent surface morphology. The root mean square (RMS) roughness is 0.09 nm for a 5 μm × 5 μm scan and 0.41 nm for an 80 μm × 80 μm scan, indicating a well-balanced strain in the active region.

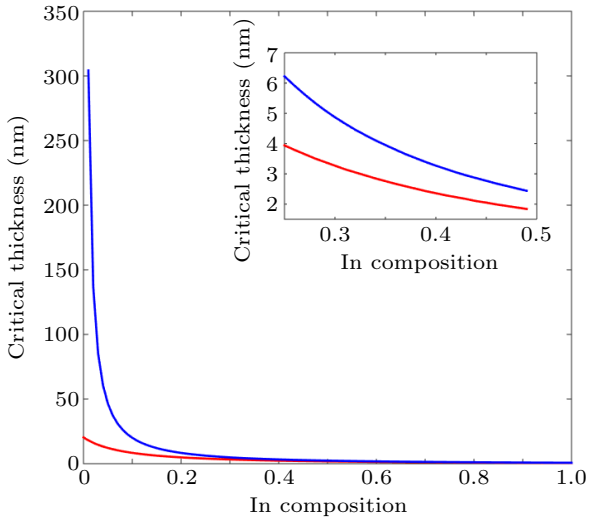


Fig. 6. Critical thickness for $Ga_{1-x}In_xSb$ as a function of x overgrown on GaSb (blue curve) and InAs (red dotted curve) substrate.

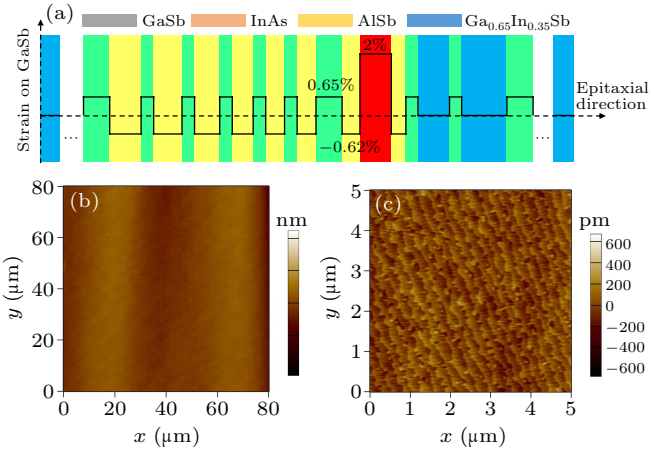


Fig. 7. (a) Schematic diagram of the active region. (b) 80 μm × 80 μm and (c) 5 μm × 5 μm AFM images for a seven-period active region overgrown on a GaSb substrate. Root mean square surface roughness values of (b) and (c) are 0.41 nm and 0.09 nm, respectively.

Adopting the strain compensation method for the thick superlattice clad layer and the complex active region, we have grown interband cascade laser structures on InAs[26] and GaSb substrates. The GaSb-based laser includes a five-period active region sandwiched by upper and lower separate-confinement layers of 0.2 μm thick GaSb and InAs/AlSb superlattice clad layers.[27,28] The high-resolution XRD spectrum, AFM and differential interference contrast (DIC) microscopy images of

the laser sample are shown in Fig. 8. Two sets of satellite peaks can be distinguished from the XRD spectrum, which comes from the InAs/AlSb superlattice clad layers and the active region, respectively. The zeroth-order satellite peak of the superlattice clad layers is located at −75 arcsec and is marked as SL(0). The zeroth-order satellite peak of the active region is difficult to distinguish from the GaSb peak. According to other symmetrically distributed satellite peaks, it is at 31 arcsec. The RMS roughness from the AFM image is 0.12 nm, and defect density from the DIC microscopy image is as low as 520 cm^{-2}.

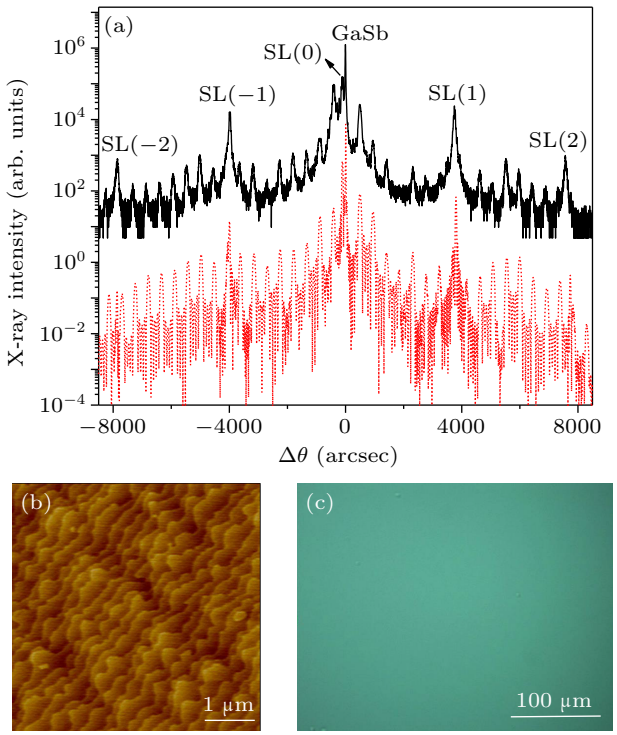


Fig. 8. High-resolution x-ray diffraction spectrum (a), AFM image (b) and DIC microscopy image (c) for a strain-compensated interband cascade laser structure.

4. Conclusion

In conclusion, we have investigated the strain compensation method for the growth of complex interband cascade laser structures. The compressive and tensile strain can be compensated by considering the balance between tensile strain energy and compressive strain energy instead of simple lattice matching. Thick InAs/AlSb superlattice layers and laser structures of high material quality were grown according to the strain compensation method. Calculation of the strain energy is based on the intrinsic parameters of the materials, including lattice constant, Poisson's ratio and shear modulus, so our proposed strain compensation method is also applicable to various coherent epitaxial material systems other than III–V semiconductors.

Acknowledgments

Project supported by the National Key Research and Development Project of China (Grant No. 2018YFB2200500), the National Natural Science Foundation of China (Grant Nos. 61790583, 61835011, 62174158 and 61991431), Youth Innovation Promotion Association of the Chinese Academy of Sciences (Grant No. 2021107), and the Key Program of the Chinese Academy of Sciences (Grant No. XDB43000000).

References

[1] Meyer J R, Bewley W W, Canedy C L, Kim C S, Kim M, Merritt C D and Vurgaftman I 2020 *Photonics* **7** 75
[2] Loghmari Z, Bahriz M, Thomas D D, Meguekam A, Nguyen Van H, Teissier R and Baranov A N 2018 *Electron. Lett.* **54** 1045
[3] Canedy C L, Bewley W W, Lindle J R, Kim C S, Kim M, Vurgaftman I and Meyer J R 2006 *J. Electron. Mater.* **35** 453
[4] Canedy C L, J Abell, Bewley W W, Aifer E H, Kim C S, Nolde J A, Kim M, Tischler J G, Lindle J R, Jackson E M, Vurgaftman I and Meyer J R 2010 *J. Vac. Sci. Technol. B* **28** C3G8
[5] Cui S N, Jiang D W, Sun J, Jia Q X, Li N, Zhang X, Li Y, Chang F R, Wang G W, Xu Y Q and Niu Z C 2020 *Chin. Phys. B* **29** 048502
[6] Jiang Z, Sun Y Y, Guo C Y, Lv Y X, Hao H Y, Jiang D W, Wang G W, Xu Y Q and Niu Z C 2019 *Chin. Phys. B* **29** 038504
[7] Cui J, Yao Y, Wang D W, Wang G W, Wang Y G, Shen X and Yu R C 2018 *J. Appl. Phys.* **124** 245301
[8] Nicolaï J, Warot-Fonrose B, Gatel C, Teissier R, Baranov A N, Magen C and Ponchet A 2015 *J. Appl. Phys.* **118** 035305
[9] Bauer A, Dallner M, Herrmann A, Lehnhardt T, Kamp M, Höfling S, Worschech L and Forchel A 2010 *Nanotechnology* **21** 455603
[10] Li L G, Liu S M, Luo S, Yang T, Wang L J, Liu F Q, Ye X L, Xu B and Wang Z G 2011 *Chin. Phys. Lett.* **28** 116802
[11] Hu Y, Tam M C and Wasilewski Z R 2019 *J. Vac. Sci. Technol. B* **37** 032902
[12] Canedy C L, Bewley W W, Boishin G I, Kim C S, Vurgaftman I, Kim M, Meyer J R and Whitman L J 2005 *J. Vac. Sci. Technol. B* **23** 1119
[13] Canedy C L, Bewley W W, Kim C S, Kim M, Vurgaftman I and Meyer J R 2003 *J. Appl. Phys.* **94** 1347
[14] Yang M J, Moore W J, Bennett B R, Shanabrook B V, Cross J O, Bewley W W, Felix C L, Vurgaftman I and Meyer J R 1999 *J. Appl. Phys.* **86** 1796
[15] Kaspi R, Lu C A, Newell T C, Yang C and Luong S 2015 *J. Crys. Growth* **424** 24
[16] Hill C J and Yang R Q 2005 *J. Crys. Growth* **278** 167
[17] Haugan H J, Brown G J, Mahalingam K, Grazulis L, Noe G T, Ogden N E and Kono J 2014 *J. Vac. Sci. Tech. B* **32** 02C109
[18] Haugan H J, Brown G J, Elhamri S, Mitchel W C, Mahalingam K, Kim M, Noe G T, Ogden N E and Kono J 2012 *Appl. Phys. Lett.* **101** 171105
[19] Haugan H J, Brown G J, Mahalingam K and Grazulis L 2015 *Infrared Phys. Techonol.* **70** 99
[20] Matthew J W and Blakeslee A E 1975 *J. Cryst. Growth* **29** 273
[21] People R and Bean J C 1985 *Appl. Phys. Lett.* **47** 322
[22] People R and Bean J C 1986 *Appl. Phys. Lett.* **49** 229
[23] Vurgaftman I, Meyer J R and Ram-Mohan L R 2001 *J. Appl. Phys.* **89** 5815
[24] Ohtani K, Beck M and Faist J 2016 *ACS Photonics* **3** 2297
[25] Nilsen T A, Breivik M, Selvig E and Fimland B O 2009 *J. Cryst. Growth* **311** 1688
[26] Yu T, Liu S, Zhang J, Xu B, Wang L, Liu J, Zhuo N, Zhai S, Ye X, Chen Y, Liu F and Wang Z 2018 *J. Semicond.* **39** 114003
[27] Yu T, Ning C, Sun R X, Liu S M, Zhang J C, Liu J Q, Wang L J, Zhuo N, Zhai S Q, Ye X L, Li Yuan and Liu F Q 2022 *AIP Adv.* **12** 015027
[28] Ning C, Yu T, Liu S, Zhang J, Wang L, Liu J, Zhuo N, Zhai S, Li Y and Liu F 2022 *Chin. Opt. Lett.* **20** 022501